Powder Metallurgy Progress, Vol.22 (2022), No.1, p.043-052
http://dx.doi.org/10.2478/pmp-2022-0006

INVESTIGATION OF HYBRID LAP WELDS OF TI6AL4V AND STAINLESS STEEL WITH BRONZE INTERLAYER

Hana Chmelíčková, Martina Havelková, Aneta Hrubantová, Vlastimil Jílek, Lukáš Václavek, Tomáš Ingr

Abstract

Welding of the austenitic stainless steel AISI 304 and Ti6Al4V is complicated by hard and brittle intermetallic compound formation. In this contribution, we study a laser welding method that partially overcomes this problem using interlayer. Bronze foil (CuSn6) of thickness 100 µm and 200 µm was inserted between steel and titanium sheets and lap welds were realized on pulsed Nd:YAG laser. Representative samples were investigated by nanohardness measurement, SEM/EDS, and XRD analysis to detect the localization of the intermetallic phases. The macrostructure of the weld cross sections was displayed by optical and digital microscopy. The nano-hardness test revealed the presence of very hard intermetallic mainly around the interface between the fusion zone and bottom metal sheet. EDS mapping displayed the main elements Fe, Cr, Cu and Ti distribution in the fusion zone, EDS line scanning detected elements` signals in the diagonal and horizontal directions. XRD analysis revealed expected intermetallic compounds FeTi and $CuTi_2$ and solid solution $Cu_{0.8}Fe_{0.2}$.

Keywords: Ti6Al4V alloy, AISI 304 stainless steel, CuSn6 interlayer, Nd:YAG welding

INTRODUCTION

The joining of the austenitic stainless steels AISI 304, 304L, or 316L and the titanium alloy Ti6Al4V is subject of the world research with the aim to overcome a problem with the large difference in physical properties of these construction materials, that causes the formation of inter-metallic compounds (IMC) not only from the main elements iron and titanium (Fe_2Ti, FeTi) but also from steel alloying elements chromium and nickel ($TiCr_2$, $NiTi_2$, Ti/Fe/Cr) [1]. High residual stresses in the inhomogeneous fusion zone cause cracks propagation through these hard and brittle IMCs. Methods of the defect-free joining of the stainless steel and Ti6Al4V were developed in several ways. Direct joining is possible with diffusion or friction welding methods far below melting temperatures [2]. Fusion joining with an electron or laser beam uses off set of the beam center to steel with the aim to melt only steel specimens and create a reactive interlayer with conduction heated titanium [3]. Another possible solution is using interlayers from metals, that have good weldability with titanium (zirconium, vanadium, niobium, molybdenum, tantalum, and

This work was presented at the conference Local Mechanical Properties 2022 held in Kosice, Slovakia on May 11-13, 2022.

Hana Chmelíčková, Vlastimil Jílek, Lukáš Václavek: Joint Laboratory of Optics of Palacký University and Institute of Physics AS CR, Faculty of Science, Palacký University in Olomouc, Joint Laboratory of Optics of Palacký University and Institute of Physics AS CR, Institute of Physics of the Academy of Sciences of the Czech Republic

Martina Havelková: Joint Laboratory of Optics of Palacký University and Institute of Physics AS CR, Institute of Physics of the Academy of Sciences of the Czech Republic

Aneta Hrubantová: Joint Laboratory of Optics of Palacký University and Institute of Physics AS CR, Faculty of Science, Palacký University in Olomouc, Department of Low-Temperature Plasma, Institute of Physics of the Czech Academy of Sciences

Tomáš Ingr: Department of Experimental Physics, Faculty of Science, Palacký University Olomouc

hafnium), but all of them are very expensive [4]. Solutions for mass production are using more accessible materials such as copper, nickel, and silver, that form with titanium less hard IMCs than Fe-Ti. Copper does not form intermetallic compounds with steel elements, its high ductility compensates difference in thermal expansion coefficients of Fe and Ti, but the strength of the joints strongly depends on various intermetallic phases in the Ti/Cu interface [5]. Known values of hardness are FeTi (~ 600 HV), Fe_2Ti (~ 1 000 HV), TiCu and Ti_2Cu_3 (998 HV – 1092 HV), Ti_2Cu (809 HV – 862 HV), Cu_4Ti_3 (917 HV – 973 HV), Cu_2Ti (408 HV – 537 HV) and Cu_4Ti (924 HV – 981 HV) [6]. The most promising method is using thin multilayers of the compatible metals with titanium (V or Nb) and Cu when the formation of Ti/Cu intermetallic is suppressed, but laser beam offset was revealed as the most critical parameter [7].

The majority of these cited experiments used butt weld configuration, the idea of our work is to examine lap joint arrangement with a thin bronze interlayer when the laser beam directly irradiates only the edge of the upper material and the other is melted or heated by thermal conduction. An influence of the pulse energy, an interlayer thickness, and the sheets' mutual position on the weld properties are tested. Inhomogeneous fusion zone properties are investigated by two microscopic methods, nanoindentation, SEM/ Energy Dispersive Spectroscopy, and X-ray diffractometry to reveal the location and amount of the intermetallic compounds.

MATERIALS AND METHODS

The austenitic stainless steel AISI 304 samples with a thickness of 0.6 mm and Ti6Al4V with a thickness of 1 mm were separated by bronze foil (CuSn6) 100 µm and 200 µm, resp. and fixed tightly on the welding jig in the lap configuration after brushing and cleaning with ethanol (Tab. 1). The laser beam in focus off set +3 mm has the theoretic diameter value 0.8 mm and it was centered to the steel upper edge with a tilt 15° from the vertical axis. Pulse frequency 13 Hz and linear axis speed 3 $mm.s^{-1}$ resulted in 70% laser spots overlap. High-purity argon was guided coaxial with a laser beam through a 2 mm nozzle with a flow rate of 12 $l.min^{-1}$. The pulse energy value was gradually set to 5.44 J, 5.58 J, 5.78 J, 5.87 J, 5.92 J, and 6.04 J, and the pulse length was set to a constant value of 3 ms, which was optimized in previous experiments. Then the mutual position of Ti6Al4V and AISI304 sheets was reversed and the experimental procedure was repeated with identical laser parameters, but the linear axis speed was set to 6 $mm.s^{-1}$ to reduce heat input to the specimen.

Tab. 1 Comparison of the selected thermo-mechanical properties of used welded materials, source https://matmatch.com/

Material	Density $kg.m^{-3}$	Hardness HV	Thermal expansion K^{-1}	Melting point K	Thermal conductivity $W.m^{-1}.K^{-1}$	Elastic modulus GPa
AISI 304	8 000	225 – 230	1.72 E^{-5}	1 728	12.2	193 – 200
Ti6Al4V	4 430	360 – 370	7.70 E^{-5}	1 947	6.7	114
CuSn6	8 820	80 – 120	1.80 E^{-5}	1 323	75	118

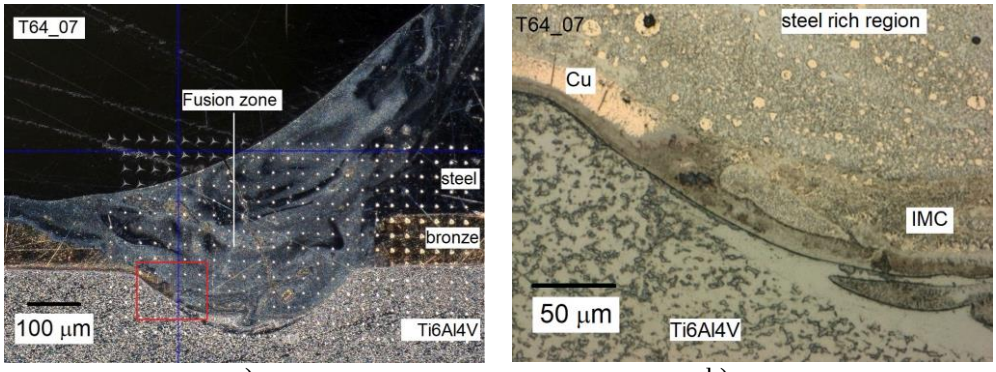
Weld macro-structure of the samples' transverse cross sections was observed using the laser scanning confocal microscope LEXT 5000 and the digital microscope KEYENCE VHX-7100. Three representative samples of each welding configuration were tested in the following methods, concretely sample T64_07 with 100 µm bronze interlayer (energy 5.58

J), T64_08 with 200 μm bronze interlayer (energy 5.87 J), and T64_04R with 100 μm bronze interlayer and reversed metal sheets position (energy 5.58 J). Nano-hardness tests of the main part of the inhomogeneous fusion zones surrounded by base materials were made using NanoTest NTX with pyramidal diamond Berkovich tip at a maximal load of 50 mN. The nanoindentation curves were evaluated by the Oliver-Pharr method for hardness and reduced elastic modulus determination. The indenter tip calibration was performed using the fused silica sample. Matrix's of (25 x 16) indents with spacing 30 μm were created and measured nanohardness values were displayed through the tables and graphs. To identify the chemical composition of the fusion zones, SEM/EDS analysis was done utilizing an SEM microscope Tescan VEGA 3 LMU. Data were displayed as EDS mapping both of the main elements Fe, Cu, and Ti and alloying elements Cr, Ni, Sn, Si, and Al too. EDS line spectra were measured in a diagonal direction across the fusion zone central part and horizontally in the interface region between the fusion zone and bottom specimen.
Intermetallic compounds Ti-Cu-Fe were characterized by X-ray diffractometry using Bragg-Brentano geometry. XRD analysis was performed on a D8 ADVANCE diffractometer (BRUKER) using Cu Kα radiation (λ = 0.154 nm) in the 2θ range 10°- 80°.

EXPERIMENTAL RESULTS AND DISCUSSION

Nanohardness test on the cross-section of the sample

The fusion zone of the sample T64_07 penetrates to titanium sheet with a maximum depth of 123 μm and a width of 443 μm at the interface level with CuSn6. Darker and lighter layers with different contents of welded metals steel and titanium alternate here due to melt pool flow. Copper is seen in the form of inclusions. The light grey region in the lowest part of the fusion zone probably contains IMC (Fig. 1(a)). Detail of this part shows copper droplets in probably a steel-rich region and a dark band of IMC on an interface with Ti6Al4V (Fig. 1(b)), where nanohardness values reached maxima from 8.18 GPa to 9.44 GPa.

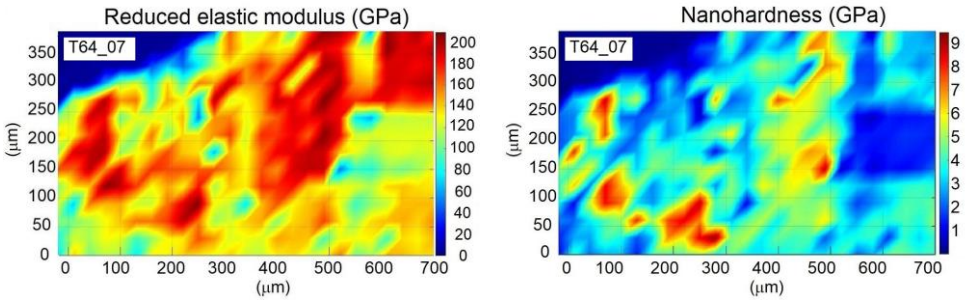


a) b)

Fig. 1. Cross section of the sample T64_07 with residual indents (a), (KEYENCE, mag. 200x); detail of the fusion zone on the bottom interface with Ti6Al4V (b), (LEXT, mag. 1200x).

Reduced elastic modulus (Er) distribution in the fusion zone of sample T64_07 was compared with the nanohardness graph (Fig. 2). There are seen individual bands of average modulus values 188 GPa, 120 GPa and 137 GPa on the right graph edge,

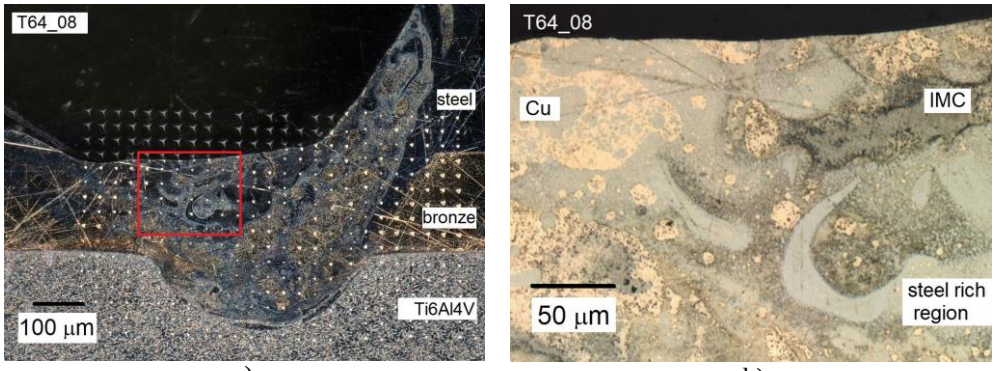
appropriate to the base materials steel, bronze and titanium alloy. Three regions with high modulus values from 184 GPa to 206 GPa occurred on the left edge of the fusion zone. The upper right part close to the bronze interlayer contains approx. 240 μm long band with module values from 182 GPa to 209 GPa (Fig. 2(a)). These high Er values mostly correspond with high nanonardness values (5.04 – 9.43) GPa and base materials positions, too (Fig. 2(b)).



a) b)

Fig. 2. Comparison of the reduced elastic modulus distribution (a) and nanohardness distribution in the fusion zone of the sample T64_07 (b).

The fusion zone of the sample T64_08 penetrates the titanium sheet with a maximum depth of 137 μm and a width of 425 μm, measured with respect to the interface CuSn6/Ti6Al4V. Copper-rich regions prevail over mixed darker and lighter layers of Fe and Ti in the right, bottom, and upper left part of the fusion zone (Fig. 3(a)). The detail of this part is displayed in Fig. 3(b). The light grey steel-rich region with copper inclusion and copper-rich region with steel inclusions surround dark inclusion with titanium, high nanohardness values from 10.22 GPa to 10.96 GPa, measured in this region, point to the occurrence of IMC.

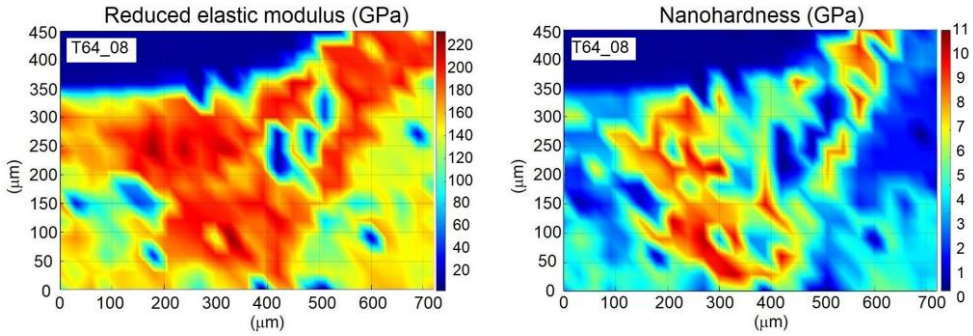


a) b)

Fig. 3. Cross section of the sample T64_08 with residual indents (a), (KEYENCE, mag. 200x); detail of the left upper part of the fusion zone (b), (LEXT, mag. 1200x).

Reduced elastic modulus (Er) distribution in the fusion zone of sample T64_08 was compared with the nanohardness graph (Fig. 4). Some blue islands with modulus

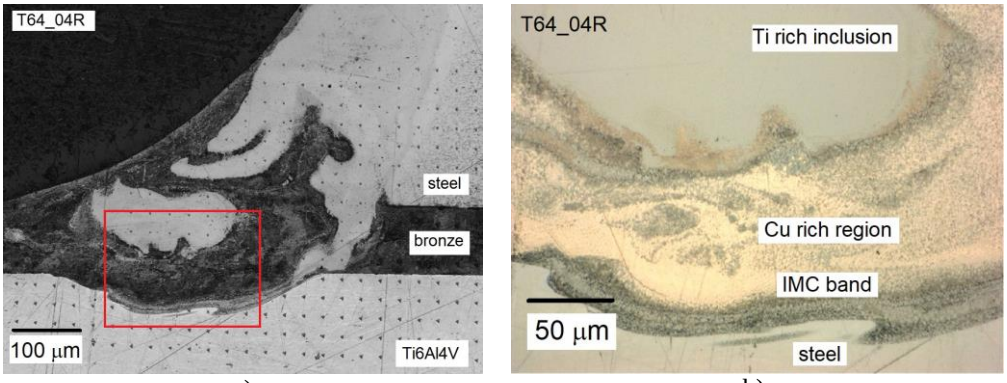
values from 25 GPa to 100 GPa are surrounded by the red range with high modulus values from 180 GPa to 228 GPa. Average values, measured behind the right edge of the fusion zone, correspond again with those of base materials, 184 GPa for steel, 125 GPa for bronze, and 137 GPa for titanium (Fig. 4(a)). The high nanohardness values from 8.03 GPa to 11.04 GPa in the left part of the fusion zone and on its interface with base materials steel and bronze correspond with high modulus values (Fig. 4(b)).



a) b)

Fig. 4. Comparison of the reduced elastic modulus distribution (a) and nanohardness distribution in the fusion zone of the sample T64_08 (b)

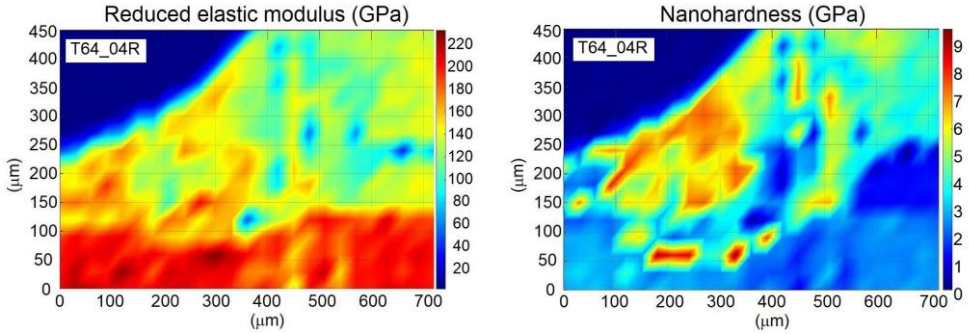
The influence of the higher welding speed and thus lower heat input on the welded materials mixing is seen on the cross-section of the sample T64_04R (Fig. 5(a)). Light grey regions with high content of the titanium are separated from the copper-rich dark region, a darker grey layered band is observable on the interface between the fusion zone and a bottom steel sheet. The detail of this part is displayed in Fig. 5(b). The copper-rich region with irregular titanium and steel scattered inclusions is surrounded by the dark band on the bottom interface with steel. The highest nanohardness values from 8.30 GPa to 9.63 GPa were measured in this region, which points to Fe–Ti intermetallic occurrence.



a) b)

Fig. 5. Cross section of the sample T64_04R with residual indents (a), (LEXT, mag. 432x); detail of the fusion zone on the bottom interface with steel (b), (LEXT, mag. 1200x)

Similarly, the reduced elastic modulus` distribution in the fusion zone of the sample T64_04R was compared with the nanohardness graph (Fig. 6). Average modulus values 134 GPa, 120 GPa, and 199 GPa on the right edge and bottom part of the graph belongs to above-mentioned base materials titanium alloy, bronze and steel, which are arranged in the reverse position against sample T64_07. The higher modulus values from 136 GPa to 191 GPa occurred in the left part of the fusion zone, they surround an area with values between 100 GPa and 120 GPa (Fig. 6(a)), where the titanium-rich island is seen in Fig. 5. The area of the same low modulus values is seen in the right upper part of the graph, where fusion zone borders on titanium alloy base material. The highest modulus values 226 GPa to 231 GPa are located in the bottom interface of the fusion zone with a steel metal sheet and correspond with the highest measured nanohardness values (8.30 – 9.63) GPa (Fig. 6(b)).

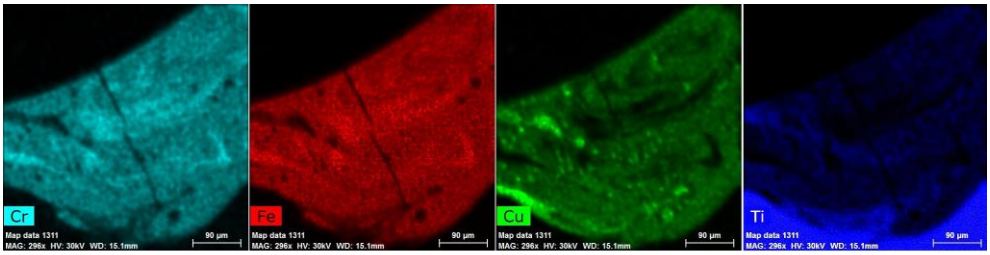


a) b)

Fig. 6. Comparison of the reduced elastic modulus distribution (a) and nanohardness distribution in the fusion zone of the sample T64_04R (b)

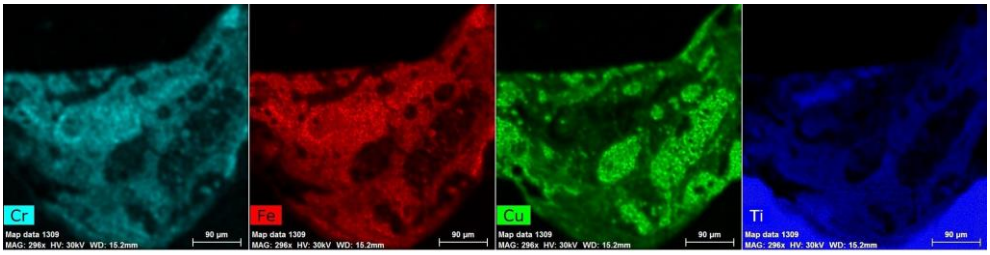
EDS mapping and line scanning, XRD analysis

The central fusion zone of sample T64_07 contains main steel elements Cr and Fe in the whole area with more intensive bands near the surface. Small, intensive islands of copper fill darker areas visible on Cr and Fe mapping. The original weak signal of titanium was lightened in the Fig. 7 to be observable mainly localized at the bottom of the fusion zone. Visible horizontal alternation of the steel-rich bands and bands with a higher copper content was caused by laser pulse overlap and repeated melting and convection of the fusion zone. Much larger separated copper-rich inclusions are observable in the case of sample T64_08 due to the twice thicker bronze interlayer. A more intensive titanium band is visible near the surface and bottom of the fusion zone (Fig. 8). Week signals of Cr and Fe are seen in the fusion zone of the sample T64_04R, where noticeably bounded areas of Cu and Ti are separated. The narrow band with high titanium content on the fusion zone bottom interface with the steel sheet is the location of the maximal nanohardness values (Fig. 9).



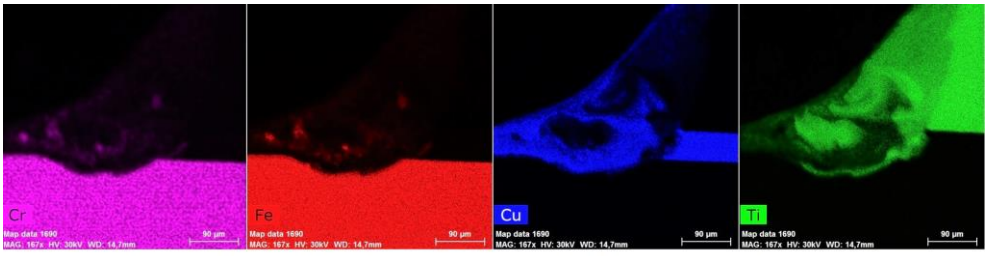
Map data 1311 MAG: 296x HV: 30kV WD: 15.1 mm scale 90 µm

Fig. 7. EDS mapping of the central fusion zone of the sample T64_07



Map data 1309 MAG: 296x HV: 30kV WD: 15.2 mm scale 90 µm

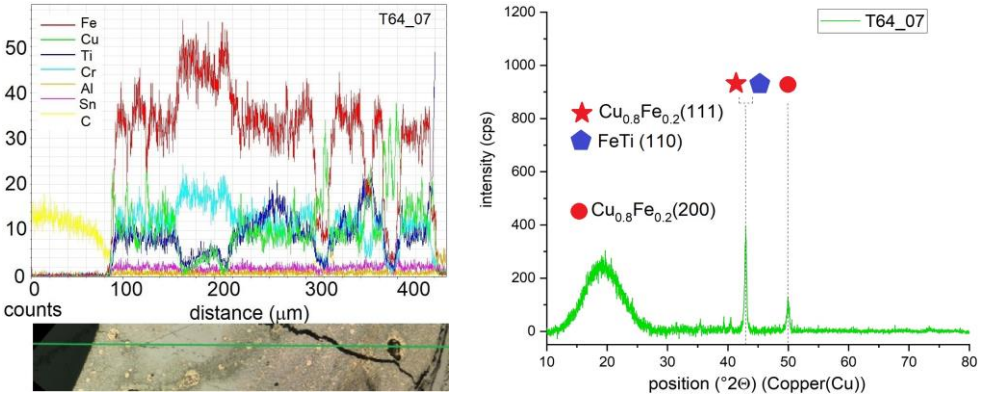
Fig. 8. EDS mapping of the central fusion zone of the sample T64_08



Map data 1690 MAG: 167x HV: 30kV WD: 14.7 mm scale 90 µm

Fig. 9. EDS mapping of the fusion zone of the sample T64_04R

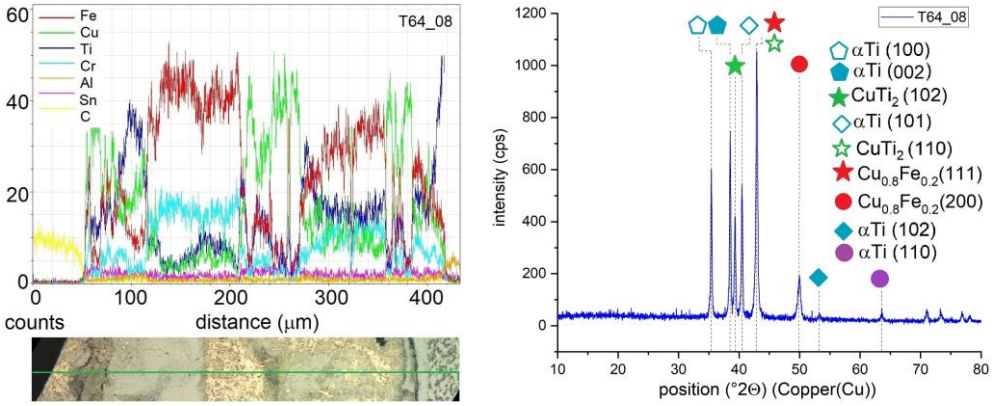
The layered structure of the T64_07 fusion zone is documented by the signal variation of Fe, Ti, Cr, and Cu in the diagonal direction across its thickest part. Relatively high signal of titanium at positions about 265 µm and 370 µm proved melting of the bottom sheet interface and mixing it to the weld pool (Fig. 10(a)). XRD analysis detected two peaks (at 43° and 50°) of the solid-state solution Cu and Fe, quenched rapidly from the melt. At 43° and 50°, $Cu_{0.8}Fe_{0.2}$ (ISCD collection code 102894), was determined and is related to the (111) and (200) crystal planes, respectively. Intermetallic phase FeTi (ICSD collection code 633925) was determined at 43° and is related to the (110) crystal plane (Fig. 10(b)).



a) b)

Fig.10. EDS line scanning across T64_07 fusion zone in the diagonal direction (a); XRD diffractogram of the sample T64_07 fusion zone (b).

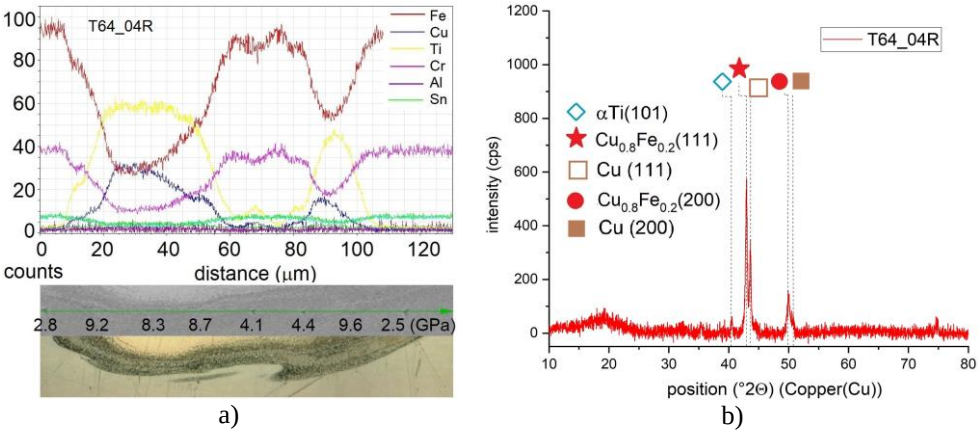
Alternation of the steel-rich and copper-rich regions in a sample T64_08 fusion zone is confirmed by Fe, Cr, and Cu counts` local maxima, EDS line scanning reveals higher signal of titanium at positions about 100 μm, 260 μm and 400 μm in the diagonal direction towards a bottom part of fusion zone (Fig. 11(a)). In a T64_08 sample fusion zone, peaks of α-titanium (ISCD collection code 253841), a solid solution of $Cu_{0.8}Fe_{0.2}$ (ICSD collection code 102894), and the intermetallic phase $CuTi_2$ (ICSD col. code 15807) were detected (Fig. 11(b)). The reflections occurred at 35.5°, 38.5°, 40.5, 53.2° and 63.6° are related to the (100), (002), (101), (102) and (110) crystal planes of α-titanium, respectively. The reflections from the $Cu_{0.8}Fe_{0.2}$ phase occur at peak positions 43.9° (111) and 50° (200). The reflections from the $CuTi_2$ phase subsist at peak positions 39.2° (102) and 43° (110).



a) b)

Fig. 11. EDS line scanning across T64_08 fusion zone in the diagonal direction (a); XRD diffractogram of the sample T64_08 fusion zone (b)

EDS line scanning across the T64_04R fusion zone bottom part in the horizontal direction connected with adequate nanohardness values shows high titanium signal in the indents 9.2 GPa, 8.3 GPa, 8.7 GP, and 9.6 GPa (Fig. 12(a)). With the reverse arrangement of the lap weld with titanium sheet on top (sample T64_04R), two times less heat input and bronze interlayer of 0.1 mm, a spectrum of $Cu_{0.8}Fe_{0.2}$ (ICSD col. code 7954) and copper (ICSD col. code 7954) can be observed, the other phases only the α – titanium (ISCD col. code 253841) is presented (Fig. 12(b)). The reflections from the $Cu_{0.8}Fe_{0.2}$ phase occur at peak positions 42.9° (111) and 50° (200), we can also determine the Cu phase at peak positions 43.8° (111) and 50.9° (200), the origin of the peak with small intensity at position 40° should correspond with α – titanium (101). Although nanohardness values are high in certain areas and indicate the presence of IMCs, their peaks may not have been intense enough.



a) b)

Fig. 12. EDS line scanning across T64_04R fusion zone bottom part in the horizontal direction (a); XRD spectra of the sample T64_04R fusion zone (b)

CONCLUSIONS

Using a bronze interlayer with a thickness of 100 μm and 200 μm, lap welds of Ti6Al4V alloy (thickness 1 mm) and austenitic stainless steel AISI 304 (thickness 0.6 mm) were created in both arrangements of the sheet positions. From the results of performed analyses, it can be concluded that the fusion zone always contained a solid solution of iron and copper, quenched rapidly from the melt, and transformed titanium. In our experiment, the local occurrence of intermetallic phases was dependent on the thickness of the interlayer and the heat input, which decreases proportionally with the increasing welding speed. Large overlapping pulses, repeated melting, and extensive melt flow resulted in the mixing of materials and intermetallic compounds formation in the fusion zone, which caused cracks.

In the case of 100 μm interlayer and heat input 24.18 $J.mm^{-1}$, areas with higher content of FeTi had much higher nanohardness and reduced elastic modulus than basic material with values higher than 9 GPa respectively 200 GPa. With a higher content of copper in the fusion zone in the case of 200 μm interlayer and heat input 25.44 $J.mm^{-1}$, distinguishable areas rich in either copper or iron were formed and the intermetallic $CuTi_2$ prevailing over FeTi were detected. Maxima of nanohardness and reduced elastic modulus are higher than 11 GPa, respectively 220 GPa.

At a higher velocity and lower heat input of 12.09 J.mm^{-1}, we observe the change in the layout of areas with similar values of nanohardness and reduced elastic modulus. It shows the permeation of the noticeably bounded areas with a predominance of titanium or copper, corresponding nanohardness and elastic modulus values are less than in previously mentioned cases. The highest values were measured only on the fusion zone interface with Ti6Al4V base material.

The fusion zone depth and internal microdefects depend not only on the laser parameters and heat input, but an important parameter is also on the inclination of the laser head and focus of the laser beam against the edge of the upper sheet. The lower sheet has to be melted to a minimal depth to limit greater penetration of its elements into the melt pool.

It has been demonstrated that with the proper setup is it possible to create a lap weld without surface cracks between otherwise incompatible materials AISI 304 and Ti6Al4V using a thin bronze interlayer.

ACKNOWLEDGMENT

The research work reported here was made possible by the continuous support of the Operational Program Research, Development, and Education, project no. CZ.02.01/0.0/0.0/17_049/0008422 of the Ministry of Education, Youth and Sports of the Czech Republic.

REFERENCES

[1] Chen, S., Zhang, M., Huang, J., Cui, C., Zhang, H., Zhao, X.: Materi. Des., vol. 53, 2014, p. 510.
[2] Tomashchuk, I., Sallamand, P.: Adv. Eng. Mater., vol. 20, 2018, p. 4.
[3] Mannucci, A., Tomashchuk, I., Mathieu, A., Cicala, E., Boucheron, T., Bolotl, R., Lafaye, S.: Procedia CIRP, vol.74, 2018, p. 490.
[4] Zhang, Y., Sun, D., Gu X., Li, H.: Mater. Lett., vol. 185, 2016, p. 152–155.
[5] Tomashchuk, I., Sallamand, P., Andrzejewski, H., Grevey, D.: Intermetallics, vol. 19, 2011, p. 1466.
[6] Mitelea, I., Groza, C., Craciunescu, C.: J. of Materi Eng and Perform, vol. 22, 2013, p. 2220.
[7] Li, J., Liu, Y., Gao, Y., Jin, P., Sun, Q., Feng, J.: Opt. Laser Technol., vol. 125, 2020, p. 8.